INTERNATIONAL JOURNAL FOR NUMERICAL METHODS IN FLUIDS
Int. J. Numer. Meth. Fluids 2003; **41**:561–576 (DOI: 10.1002/fld.452)

Elastohydrodynamics of tensioned web roll coating process

M. S. Carvalho*,†

Department of Mechanical Engineering, Pontifícia Universidade Católica do Rio de Janeiro, Rua Marquês de São Vicente, 225, Gávea, Rio de Janeiro, RJ 22453-900, Brazil

SUMMARY

Coating process is an important step in the manufacturing of different products, such as paper, adhesive and magnetic tapes, photographic films, and many other. The tensioned web roll coating is one the several methods used by different industries. It relies on the elastohydrodynamic action between the fluid and the tensioned substrate for transferring and applying the liquid. The main advantage of this method is its ability to apply very thin liquid layers with less sensitivity to mechanical tolerance at relative small cost. Despite its industrial application, theoretical analysis and fundamental understanding of the process are limited. This work analyses this elastohydrodynamic action by solving the differential equations that govern the liquid flow, described by the Navier–Stokes equation, and the web deformation, modelled by the cylindrical shell approximation. The goal is to determine the operating conditions at which the process is two dimensional and defect free. The equations are discretized by the Galerkin/finite-element method. The resulting non-linear system of equations is solved by Newton's method coupled with pseudo-arc-length continuation in order to obtain solutions around turning points. The theoretical results are used to construct an operating window of the process that is in agreement with limited experimental data. Copyright © 2003 John Wiley & Sons, Ltd.

KEY WORDS: elastohydrodynamics; coating process; tensioned web; finite-element method

1. INTRODUCTION

In industrial coating processes, one or several liquid layers are deposited on a substrate and are then dried to form a solid film that serves a specific function. This process is vital in the manufacturing of different products, like paper, adhesive and magnetic tapes, magnetic disks, photographic films, and many others. The different ways of depositing a liquid on the substrate lead to different coating methods. Some of these methods rely on the interaction between hydrodynamic forces exerted by the flowing coating liquid and forces exerted by a deformable solid boundary that confines the flow, i.e. an elastohydrodynamic interaction.

* Correspondence to: M. S. Carvalho, Department of Mechanical Engineering, Pontifícia Universidade Católica do Rio de Janeiro, Rua Marquês de São Vicente 225, Gávea, Rio de Janeiro, RJ 22453-900, Brazil.
† E-mail: msc@mec.puc-rio.br

Contract/grant sponsor: CNPq (Brazilian Research Council); contract/grant number: 300242/98-0

Received 12 February 2002
Revised 10 September 2002

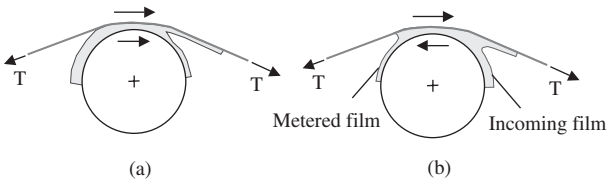

Figure 1. Tensioned web roll coating process: (a) forward mode, (b) reverse mode.

Elastohydrodynamic coating systems include flexible blade, membrane coaters, squeeze roll, gravure coaters, tensioned web roll and slot coaters. Pranckh and Coyle [1] presented a detailed analysis of these different coating systems. The main advantage of elastohydrodynamic coating methods is their ability to apply very thin liquid layers with less sensitivity to mechanical tolerances at a relative small cost, when compared to more sophisticated pre-metred coating methods, such as slot, slide and curtain coating. However, poor quality of the substrate, such as variation in its thickness, bagginess and any other non-uniformities tend to degrade the coating quality.

One of the many examples of elastohydrodynamic coating systems, the tensioned web roll coating uses only the deformable substrate without any external mechanical support to provide the elastic boundary for the liquid flow and to impose load in the coating bead. The liquid is transferred to the substrate as it passes over a rotating roll, as illustrated in Figure 1. The roll and the substrate can be moving in the same direction, i.e. forward mode, or in opposite directions, called a reverse mode.

This work analyses the flow in a tensioned web roll coating bead operating in the reverse mode, as shown in Figure 1(b). The liquid is brought to the bead as a layer in the applicator roll, referred as the incoming layer. It is supplied to the roll by dip coating or by a slot die located upstream the coating bead. Part of the liquid is transferred to the substrate and the remaining stays on the roll creating what is usually called the metred film. The film thickness transferred to the web is a function of the roll and web speeds, liquid viscosity, substrate stiffness and tension, and the wrapping angle of the substrate over the rotating roll. It is important to understand this elastohydrodynamic action in order to be able to predict and optimize this important industrial process.

When the substrate wraps part of the rotating roll, an elongated channel with virtually uniform height is formed between the two moving surfaces. The flow in this region is close to a Couette flow because the pressure gradient approaches zero. Therefore, the flow rate between the roll and the substrate, and consequently the film thickness transferred to the web, can be determined by the channel height (unknown *a priori*), roll and web velocity.

The first analysis of the distance between a moving tensioned membrane and a rigid roll with viscous liquid flowing between them was done by Blok and Van Rossum [2]. They measured the thickness of a lubricating oil layer between a thin cellophane foil and a cylinder. Using a simplified analysis, they derived an expression for the oil thickness H_0:

$$H_0 = 0.426 R_0 \left(6 \frac{\mu V}{T} \right)^{2/3}$$

where, R_0 is the cylinder radius, μ is the fluid viscosity, V is the web speed and T the tension of the web. Eshel and Elrod [3] developed a theoretical model using Reynolds equation of

lubrication to describe the fluid flow with the assumptions of fluid incompressibility, and infinitely wide foil of negligible stiffness. The relationship between the fluid thickness and operating parameters they derived is

$$H_0 = 0.643 R_0 \left(6 \frac{\mu V}{T} \right)^{2/3}$$

The relation derived by Eshel and Elrod can only be used as an estimate for the film thickness between the web and the roll in a tensioned web roll coater. It does not take into account details of the free surface flow. Despite its important industrial application, theoretical analysis of this process is limited to lubrication type analysis. In this work, the liquid flow is described by the full Navier–Stokes equation with appropriate boundary conditions at the free surface that include capillary effects. The deformation of the substrate is modelled by the cylindrical shell approximation. The goal is to determine the metred film thickness, and consequently the transferred film thickness, as a function of the operating parameters, and the operating conditions at which the process is two-dimensional and defect free. The differential equations that govern the liquid flow and the substrate deformation are discretized by the Galerkin/finite-element method. The resulting non-linear system of equations is solved by Newton's method coupled with pseudo-arc-length continuation in order to obtain solutions around turning points. The theoretical results are used to construct an operating window for the process that is in agreement with some experimental data available.

2. ELASTOHYDRODYNAMIC MODEL

2.1. Governing equations

The configuration of the problem analysed in this work is illustrated in Figure 2.

The roll that brings the liquid into the transfer region is moving from right to left in the figure. The substrate is moving in the opposite direction and takes part of the liquid with it. The remaining liquid stays on the roll and is later removed from it by a scraper, not analysed here. The liquid traction deforms the tensioned substrate. The flow and the deformation are coupled in what is called *elastohydrodynamic behaviour*.

It is important to characterize the position of the moving roll relative to the upstream and downstream idlers that guide the moving web. The relative position can be characterized by the distance ΔY from the top of the roll to the axis that passes through the idlers, called here the x-axis. The co-ordinate $x = 0$ is defined in the plane that passes through the centre of the roll, as indicated in the figure. When $\Delta Y < 0$, the web does not touch the roll. When $\Delta Y > 0$, the web wraps around a portion of the roll. The substrate is assumed to be infinitely wide, and

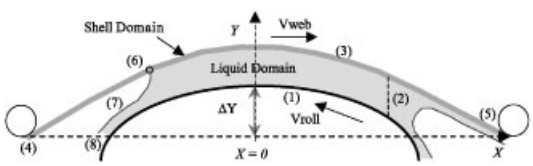

Figure 2. Sketch of domain of calculation with liquid and shell domain. At $\Delta Y/R > 0$, the web wraps the roll, and at $\Delta Y/R < 0$, it does not touch the roll surface when at rest.

therefore the flow in the transverse direction is neglected. The motion of the liquid is described by the Navier–Stokes equation and continuity equation for incompressible Newtonian fluid:

$$\rho \underline{v} \cdot \nabla \underline{v} - \nabla \cdot [-p\underline{\underline{I}} + \mu(\nabla \underline{v} + (\nabla \underline{v})^{\mathrm{T}})] \quad \text{and} \quad \nabla \cdot \underline{v} = 0 \tag{1}$$

together with appropriate boundary conditions. ρ and μ are the liquid density and viscosity, respectively. The deformation of the web is modelled by the equations of cylindrical shells (see Reference [4]):

$$\left.\begin{aligned} \frac{\mathrm{d}T}{\mathrm{d}\xi} + \kappa \frac{\mathrm{d}}{\mathrm{d}\xi}(\kappa D) + P_t &= 0 \\ -\frac{\mathrm{d}^2}{\mathrm{d}\xi^2}(\kappa D) + \kappa T + P_n &= 0 \\ \frac{\mathrm{d}^2 x}{\mathrm{d}\xi^2} + \kappa \frac{\mathrm{d}y}{\mathrm{d}\xi} = 0 \quad \text{or} \quad \frac{\mathrm{d}^2 y}{\mathrm{d}\xi^2} - \kappa \frac{\mathrm{d}x}{\mathrm{d}\xi} &= 0 \end{aligned}\right\} \tag{2}$$

ξ is the co-ordinate along the web. T and κ are the web tension and curvature at each position, and x and y are the Cartesian co-ordinates of points on the web. The web stiffness $D \equiv Et^3/12(1-v^2)$ is a function of the elastic modulus E, Poison ratio v, and thickness of the web t. P_t and P_n are the loading forces on the web in the tangential and normal direction.

The domain of calculation is divided into two different subdomains: One where the Navier–Stokes equation is solved (Ω_f), and the other where the cylindrical shell equations are solved (Ω_s).

The goal of this work is to analyse the amount of liquid that remains on the roll, i.e. the metred film thickness, at different operating conditions. Because this process usually runs in a flooded condition, and this work is only interested in the behaviour of the metred film, the flow near the free surface in the upstream side of the coating gap is not considered. In the analysis presented here, it is substituted by what is called a flooded inlet, i.e. an artificial boundary condition used to reduce the side of the domain of calculation, plane (2) shown in Figure 2. The boundary conditions used to integrate the partial differential equations (1) and (2) are described next.

At the roll surface (1), the no-slip and no-penetration conditions apply, viz.,

$$\underline{v} = \underline{V}_{\mathrm{roll}} \tag{3a}$$

The artificial boundary (2) that limits the fluid domain is located far enough from the narrow channel between the roll and the substrate that its location had no effect on the predictions reported here. On that position, the liquid pressure was assumed to be atmospheric:

$$p = P_0 \tag{3b}$$

At the interface between the coating liquid and the flexible substrate (3), the liquid velocity is equal to the web velocity, viz.,

$$\underline{v} = \underline{V}_{\mathrm{web}} \tag{3c}$$

and the loading force responsible for the web deformation is the traction exerted by the fluid. Underneath the web, the traction vector is

$$P_t = -\underline{t} \cdot (\underline{n} \cdot \underline{\underline{\sigma}}) \quad \text{and} \quad P_n = -\underline{n} \cdot (\underline{n} \cdot \underline{\underline{\sigma}}) \tag{3d}$$

$\underline{\underline{\sigma}}$ is the Cauchy stress tensor, $\underline{t}$ and $\underline{n}$ are the tangential and normal unitary vectors.

In one extreme of substrate (4), the position, curvature and web tension have to be specified:

$$\underline{x} = \underline{X}_{\text{up}}; \quad \kappa = 0; \quad \text{and} \quad T = T_{\text{up}} \tag{3e}$$

In the other extreme (5), only the position and curvature are specified:

$$\underline{x} = \underline{X}_{\text{down}}; \quad \text{and} \quad \kappa = 0 \tag{3f}$$

At the free surface (7), the traction in the liquid balances the capillary pressure and there is no mass flow across the gas–liquid interface:

$$\underline{n} \cdot \underline{\underline{\sigma}} = \sigma \frac{\mathrm{d}\underline{t}}{\mathrm{d}s} - \underline{n} P_{\text{a}} \quad \text{and} \quad \underline{n} \cdot \underline{v} = 0 \tag{3g}$$

$\underline{t}$ is the unit vector tangent to the interface, σ is the liquid surface tension, and P_{a} is the pressure of the air, assumed atmospheric.

At the synthetic outflow plane (8), the usual boundary condition of zero traction in the normal direction cannot be applied. The pressure at the outflow plane is larger than atmospheric, because of the small curvature of the free surface. Its value depends on the film thickness and therefore it is unknown *a priori*. A more appropriate boundary condition is to set the directional derivative of velocity to zero:

$$\underline{n} \cdot \nabla \underline{v} = 0 \tag{3h}$$

At the dynamic contact line (6), the Navier slip condition was used instead of the no-slip condition and a dynamic contact angle θ_{d} was imposed:

$$\frac{1}{\beta} \underline{t}_w \cdot (\underline{v} - \underline{V}_w) = \underline{t}_w \cdot (\underline{n}_w \cdot \underline{\underline{\sigma}}) \quad \text{and} \quad \underline{n}_w \cdot \underline{n}_{fs} = \cos(\theta_{\text{d}}) \tag{3i}$$

The relevant variables can be combined into the following dimensionless groups:
Reynolds number

$$Re \equiv \frac{\rho V_{\text{roll}} R}{\mu}$$

Tension number

$$\tau \equiv \frac{\mu V_{\text{roll}}}{T}$$

Elasticity number

$$Es \equiv \frac{D}{TR^2} = \frac{Et^3}{12(1-\nu^2)TR^2}$$

Speed ratio

$$S \equiv \frac{V_{\text{web}}}{V_{\text{roll}}}$$

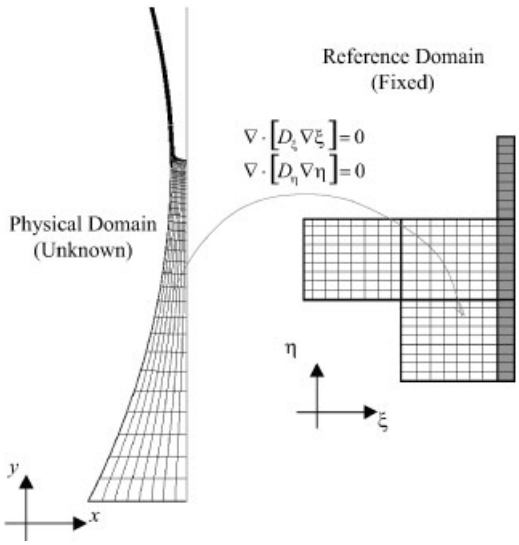

Figure 3. Mapping from the physical unknown domain to the reference fixed domain.

Wrapping angle

$$\alpha \equiv \frac{\Delta Y}{R}$$

Capillary number

$$\frac{\mu V_{\text{roll}}}{\sigma}$$

The Reynolds number gives the ratio of inertial to viscous forces. The Tension number characterizes the ratio between the viscous force (pressure) action on the web to the tension that is applied on it. The elasticity number is the ratio between the moment required to bend the web to the moment of the tension about the centre of the roll. Because the radius of the roll is large and the substrate thickness small, the elasticity number for the situation explored here are very small, in the order of 10^{-12}. The wrapping angle characterizes the relative position of the roll to the web.

2.2. Solution method

The governing equations and the boundary conditions, Equations (1)–(3), give rise to a *free boundary problem*. The location of the moving web and the liquid/air interface are unknown *a priori*. Details of treating viscous free surface problems were given by Kistler and Scriven [5, 6] and Sackinger *et al.* [7]. The basis of the solution method is recounted briefly here together with the specifics of dealing with liquid/shell interaction.

In order to solve a free boundary problem using standard techniques for boundary value problems, the set of differential equations posed in the unknown physical domain has to be transformed to an equivalent set defined in a known, fixed reference domain, as sketched in Figure 3. This approach has been extensively used to solve viscous flow with liquid/air interface (see Reference [6]). In that class of problem, the position of the liquid/air interface

is implicitly located by imposing the kinematic boundary condition at the interface. In the situation studied here, the position of the web is implicitly located by imposing the system of ordinary differential equations (2).

The transformation of the set of differential equations that governs the problem is made by a mapping $\underline{x} = \underline{x}(\underline{\xi})$ that connects the physical domain, parameterized by the position vector $\underline{x}$, and reference domain, parameterized by $\underline{\xi}$. The inverse of the mapping $\underline{x} = \underline{x}(\underline{\xi})$ used here is governed by a pair of elliptic differential equations identical with those encountered in the dilute regime of diffusional transport, as presented by de Santos [8]. The co-ordinate potentials ξ and η satisfy

$$\nabla \cdot (D_\xi \nabla \xi) = 0 \quad \text{and} \quad \nabla \cdot (D_\eta \nabla \eta) = 0 \tag{4}$$

D_ξ and D_η are the diffusion coefficients. They control the spacing of the curves of constant ξ and η chosen to tessellate the domain. The discrete version of the mapping equation is generally referred to as mesh generation equations.

The Navier–Stokes equation (1), the substrate deformation (2) and the mesh generation equations (4) together with the respective boundary conditions were solved by the Galerkin's method with quadrilateral and linear finite elements. Biquadratic basis functions ϕ_i were used to represent both the velocity and the mapping from the reference to the physical domain. The basis functions ψ_i used to represent the pressure field were piecewise, linear and discontinuous. The tension and curvature of the substrate were represented by one-dimensional quadratic basis functions φ_i, defined only along the one-dimensional elements used to represent the substrate:

$$u = \sum_{j=1}^{n} U_j \phi_j; \quad v = \sum_{j=1}^{n} V_j \phi_j; \quad p = \sum_{j=1}^{m} P_j \psi_j$$

$$x = \sum_{j=1}^{n} X_j \phi_j; \quad y = \sum_{j=1}^{n} Y_j \phi_j$$

$$T = \sum_{j=1}^{l} T_j \varphi_j; \quad \kappa = \sum_{j=1}^{l} K_j \varphi_j$$

The coefficients of the basis functions were the unknowns of the problem. They had to satisfy the equations that made the weighted residuals of Galerkin's method vanish. Those weighted residuals written in the reference domain Ω_0 were

$$R_i^{M_x} = \iint_{\Omega_0} \left\{ Re\, \phi_i \left(u \frac{\partial u}{\partial x} + v \frac{\partial u}{\partial y} \right) + \frac{\partial \phi_i}{\partial x} \left(-p + 2 \frac{\partial u}{\partial x} \right) + \frac{\partial \phi_i}{\partial y} \left(\frac{\partial u}{\partial y} + \frac{\partial v}{\partial x} \right) - St\ g_x \phi_i \right\} |\underline{\underline{J}}|\, d\Omega_0 - \int_{\Gamma_0} \phi_i (\underline{n} \cdot \underline{\underline{\sigma}})_x \left(\frac{d\Gamma}{d\Gamma_0} \right) d\Gamma_0 \tag{5a}$$

$$R_i^{M_y} = \iint_{\Omega_0} \left\{ Re\, \phi_i \left(u \frac{\partial v}{\partial x} + v \frac{\partial v}{\partial y} \right) + \frac{\partial \phi_i}{\partial x} \left(\frac{\partial u}{\partial y} + \frac{\partial v}{\partial x} \right) + \frac{\partial \phi_i}{\partial y} \left(-p + 2 \frac{\partial v}{\partial y} \right) - St\, g_y \phi_i \right\} |\underline{\underline{J}}|\, d\Omega_0 - \int_{\Gamma_0} \phi_i (\underline{n} \cdot \underline{\underline{\sigma}})_y \left(\frac{d\Gamma}{d\Gamma_0} \right) d\Gamma_0 \tag{5b}$$

$$R_i^c = \iint_{\Omega_0} \left(\frac{\partial u}{\partial x} + \frac{\partial v}{\partial y} \right) \psi_i |\underline{\underline{J}}| \, \mathrm{d}\Omega_0 \tag{5c}$$

$$\begin{aligned} R_i^x = &- \iint_{\Omega_0} D_\xi \left(\frac{\partial y}{\partial \eta} \frac{\partial \phi_i}{\partial x} - \frac{\partial x}{\partial \eta} \frac{\partial \phi_i}{\partial y} \right) \mathrm{d}\Omega_0 \\ &+ \int_{\Gamma_0} D_\xi \frac{1}{|\underline{\underline{J}}|} \left(\frac{\partial y}{\partial \eta} n_x - \frac{\partial x}{\partial \eta} n_y \right) \phi_i \left(\frac{\mathrm{d}\Gamma}{\mathrm{d}\Gamma_0} \right) \mathrm{d}\Gamma_0 \end{aligned} \tag{5d}$$

$$\begin{aligned} R_i^y = &- \iint_{\Omega_0} D_\eta \left(-\frac{\partial y}{\partial \xi} \frac{\partial \phi_i}{\partial x} + \frac{\partial x}{\partial \xi} \frac{\partial \phi_i}{\partial y} \right) \mathrm{d}\Omega_0 \\ &+ \int_{\Gamma_0} D_\eta \frac{1}{|\underline{\underline{J}}|} \left(-\frac{\partial y}{\partial \xi} n_x + \frac{\partial x}{\partial \xi} n_y \right) \phi_i \left(\frac{\mathrm{d}\Gamma}{\mathrm{d}\Gamma_0} \right) \mathrm{d}\Gamma_0 \end{aligned} \tag{5e}$$

$|\underline{\underline{J}}| \equiv \det(\underline{\underline{J}}) = (\partial x/\partial \xi)\partial y/\partial \eta - (\partial y/\partial \xi)\partial x/\partial \eta$ is the *Jacobian of the transformation* from the physical domain to the reference domain.

Along the liquid/gas meniscus, the x- or y-mapping weighted residual are replaced by the kinematic condition. The corresponding weighted residual is

$$R_i^x \text{ or } R_i^y = \int_{\Gamma_0} (\underline{n} \cdot \underline{v}) \phi_i \frac{\mathrm{d}\Gamma}{\mathrm{d}\Gamma_0} \, \mathrm{d}\Gamma_0.$$

Along the free surface, the boundary integrals in the weighted residuals of the x- and y-components of the momentum equation that come from the divergence theorem become

$$-\int_{\Gamma_0} \phi_i (\underline{n} \cdot \underline{\underline{\sigma}})_x \left(\frac{\mathrm{d}\Gamma}{\mathrm{d}\Gamma_0} \right) \mathrm{d}\Gamma_0 = \int_{\Gamma_0} \left\{ P_\mathrm{a} \phi_i n_x \frac{\mathrm{d}\Gamma}{\mathrm{d}\Gamma_0} + \sigma t_x \frac{\mathrm{d}\phi_i}{\mathrm{d}\Gamma_0} \right\} \mathrm{d}\Gamma_0 - \sigma \phi_i t_x |_b^e$$

$$-\int_{\Gamma_0} \phi_i (\underline{n} \cdot \underline{\underline{\sigma}})_y \left(\frac{\mathrm{d}\Gamma}{\mathrm{d}\Gamma_0} \right) \mathrm{d}\Gamma_0 = \int_{\Gamma_0} \left\{ P_\mathrm{a} \phi_i n_y \frac{\mathrm{d}\Gamma}{\mathrm{d}\Gamma_0} + \sigma t_y \frac{\mathrm{d}\phi_i}{\mathrm{d}\Gamma_0} \right\} \mathrm{d}\Gamma_0 - \sigma \phi_i t_y |_b^e$$

Along the liquid/web interface, the free boundary is implicitly located by substituting the x- or y-mapping weighted residual by the system of equations of cylindrical shells. The corresponding set of weighted residuals is

$$R_i^\mathrm{T} = \int_{\Gamma_0} \phi_i \left\{ \frac{\mathrm{d}T}{\mathrm{d}\Gamma_0} + D\kappa \frac{\mathrm{d}\kappa}{\mathrm{d}\Gamma_0} + (\underline{n} \cdot \underline{\underline{\sigma}}) \cdot \underline{t} \frac{\mathrm{d}\Gamma}{\mathrm{d}\Gamma_0} \right\} \mathrm{d}\Gamma_0$$

$$R_i^\kappa = \int_{\Gamma_0} \left\{ D \frac{\mathrm{d}\kappa}{\mathrm{d}\Gamma_0} \frac{\mathrm{d}\phi_i}{\mathrm{d}\Gamma_0} \frac{\mathrm{d}\Gamma_0}{\mathrm{d}\Gamma} + \kappa T \phi_i \frac{\mathrm{d}\Gamma}{\mathrm{d}\Gamma_0} + (\underline{n} \cdot \underline{\underline{\sigma}}) \cdot \underline{n} \phi_i \frac{\mathrm{d}\Gamma}{\mathrm{d}\Gamma_0} \right\} \mathrm{d}\Gamma_0$$

$$R_i^x \text{ or } R_i^y = -\int_{\Gamma_0} \left(\frac{\mathrm{d}y}{\mathrm{d}\Gamma_0} \frac{\mathrm{d}\phi_i}{\mathrm{d}\Gamma_0} \frac{\mathrm{d}\Gamma_0}{\mathrm{d}\Gamma} + \kappa \phi_i \frac{\mathrm{d}x}{\mathrm{d}\Gamma_0} \right) \mathrm{d}\Gamma_0$$

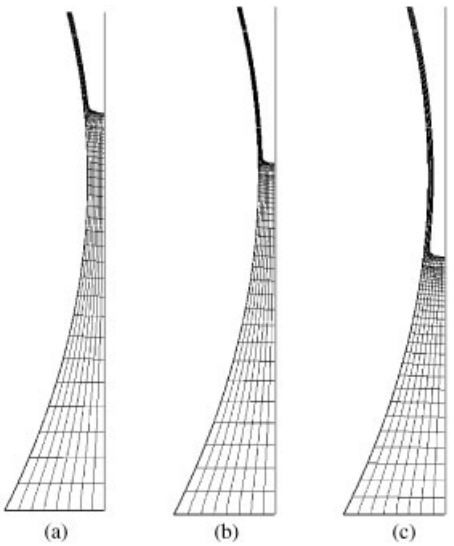

Figure 4. Domain configuration with respective mesh at rising speed ratio: (a) $S=0.6$, (b) $S=0.7$, and (c) $S=0.8$. $\mathrm{Ca}=0.1$, $\Delta Y/R=-10^{-3}$ and $\tau=10^{-6}$.

The x- and y-momentum weighted residuals along the substrate are replaced by the no-slip/no-penetration condition. The corresponding weighted residuals are

$$R_i^{M_x}=\int_{\Gamma_0}(\underline{n}\cdot\underline{v})\phi_i\,\frac{\mathrm{d}\Gamma}{\mathrm{d}\Gamma_0}\,\mathrm{d}\Gamma_0$$

$$R_i^{M_y}=\int_{\Gamma_0}(\underline{t}\cdot\underline{v}-\underline{V}_{\mathrm{web}})\phi_i\,\frac{\mathrm{d}\Gamma}{\mathrm{d}\Gamma_0}\,\mathrm{d}\Gamma_0$$

Along the portion of the substrate not attached to the flow, i.e. the portion upstream of the dynamic contact line, the tension, curvature and position of the substrate are determined in the same way as explained above. The only difference is that the terms corresponding to the liquid traction are not considered.

The resulting non-linear system of algebraic equations for the coefficients of the basis functions were solved by Newton's method. The domain was divided into 484 elements with 9144 unknowns. Each solution took approximately 5 min to be computed in a Pentium III processor. Figure 4 shows representative meshes with $\Delta Y<0$, i.e. the substrate is not wrapped around the roll.

In order to obtain solutions at large wrapping angles, i.e. large values of ΔY, a good initial guess is vital. The procedure adopted was to first obtain solutions with the roll far from the web, i.e. $\Delta Y<0$. At these conditions, the pressure that builds up in the liquid is small leading to extremely small web deformation. The only unknown boundary is the liquid/air meniscus. After a solution is computed, a first-order, arc-length continuation on the position of the roll was used to obtain solutions at the relevant set of parameters and to determine turning points on the solution path.

3. THEORETICAL PREDICTIONS

The clearance between the web and the roll is very small, and therefore the predictions are presented for vanishing Reynolds number. The tension number was kept fixed at $\tau = 10^{-6}$ in all calculations. This is a characteristic value for coating applications with polymeric substrates.

The domain configuration of a sequence of solutions at $\mathrm{Ca} = 0.1$, $\Delta Y/R = -10^{-3}$, $\tau = 10^{-6}$ and rising speed ratio is shown in Figure 4. When the substrate is far the rotating roll, the flow behaviour is similar to that of reverse roll coating (see References [9, 10]). As the web speed increases, the dynamic contact line is pulled close and then through the plane of minimum distance between the roll and the substrate ($x = 0$). This behaviour occurs at all Capillary numbers, as illustrated in Figure 5.

The conditions at which the contact line crosses the plane $x = 0$ can be related with the onset of the *seashore instability*, as explained by Coyle *et al.* [9].

The metred film thickness at all the flow states shown in Figure 5 is plotted in Figure 6. First the film thickness decreases as the speed ratio is raised: As the web speed increases, the substrate carries more liquid with it and less liquid is left on the roll surface. Moreover, as the meniscus is pulled close to the $x = 0$ plane, the radius of curvature of the meniscus falls and consequently, the pressure underneath the free surface becomes more and more negative, as illustrated in Figure 7.

The adverse pressure gradient along the metred film, as it emerges from the meniscus, rises, leading to a smaller film thickness. However, above the speed ratio at which the dynamic contact line passes through the $x = 0$ plane, the behaviour of the metred film changes, its thickness increases with speed ratio. After the meniscus has passed through the $x = 0$ plane, its radius of curvature rises with speed ratio, the pressure underneath the meniscus becomes less negative, and the adverse pressure gradient on the film less severe, leading to larger film thicknesses. At each Capillary number there is a minimum metred film thickness possible.

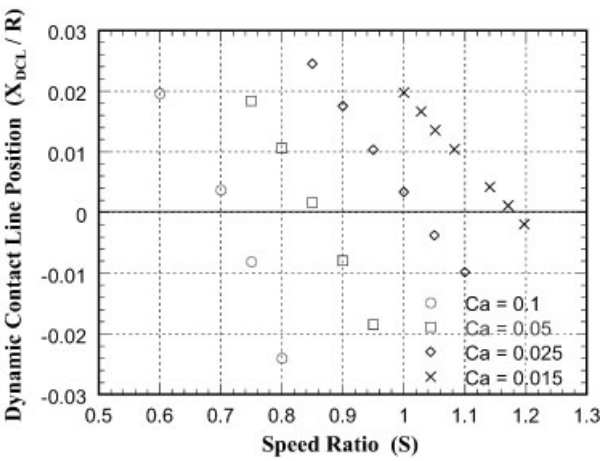

Figure 5. Dynamic contact line as a function of speed ratio and capillary number. $\Delta Y/R = -10^{-3}$ and $\tau = 10^{-6}$.

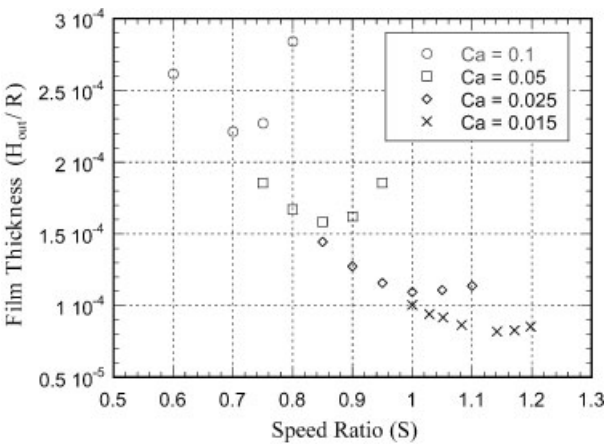

Figure 6. Thickness of metred film as a function of speed ratio and capillary number. $\Delta Y/R = -10^{-3}$ and $\tau = 10^{-6}$.

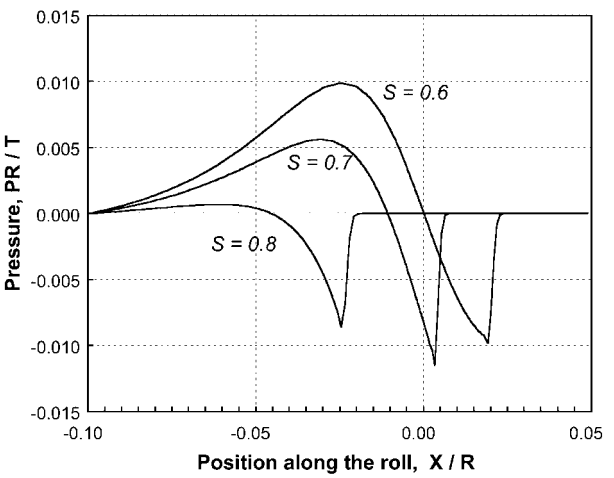

Figure 7. Pressure along the roll at different speed ratio. Ca = 0.1.

When tensioned web is used to transfer a film to a substrate, it is desired to transfer all or most of the liquid deposited on the roll. Therefore, the metred film thickness has to approach zero. As it is clear from Figure 6, this cannot be achieved with the configuration where the web is not wrapping part of the roll. The effect of pushing the roll against the substrate is examined next. Figure 8 shows the domain configuration of a sequence of flow states as the roll is pushed against the web. The Capillary number was Ca = 0.1 and the speed ratio $S = 0.7$. As expected, the substrate becomes more and more deformed. The free surface profile of these flow states is presented in Figure 9. As the roll is pushed against the substrate, the dynamic contact line and the meniscus moves away from the $x = 0$ plane.

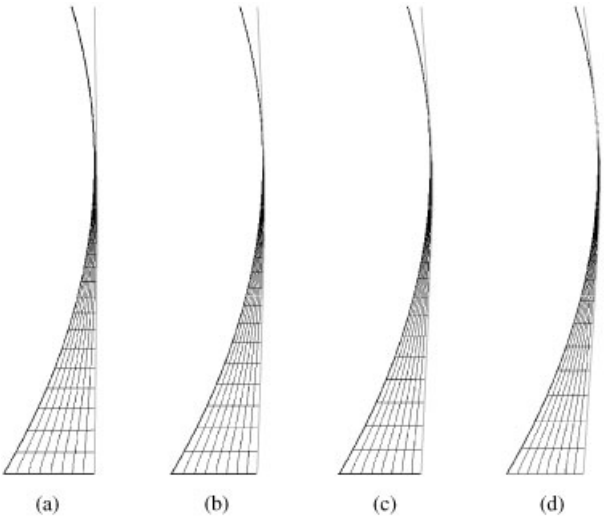

Figure 8. Domain configuration with respective mesh at different wrapping angle: (a) $\Delta Y/R = 0$, (b) $\Delta Y/R = 3 \times 10^{-4}$, (c) $\Delta Y/R = 5 \times 10^{-4}$ and (d) $\Delta Y/R = 8 \times 10^{-4}$. Ca $= 0.1$, $S = 0.7$, and $\tau = 10^{-6}$.

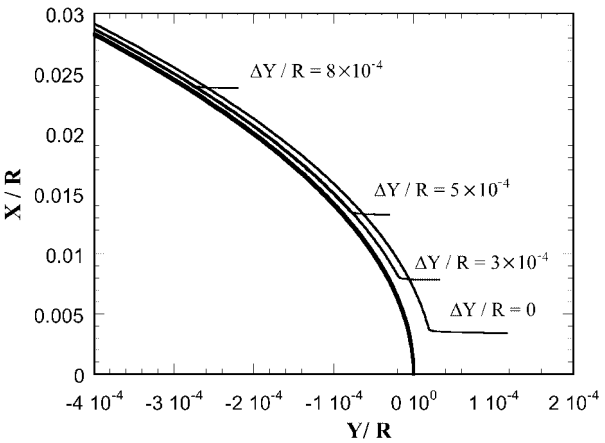

Figure 9. Free surface profile as a function of wrapping angle: Ca $= 0.1$, $S = 0.7$ and $\tau = 10^{-6}$.

The metred film thickness at different wrapping angles and speed ratio is shown in Figure 10. At small wrapping angles, i.e. $\Delta Y/R < 10^{-4}$, as in the cases when the web does not wrap the roll, flow states could be computed at all speed ratio, and there was a minimum thickness. It occurred at the speed ratio at which the dynamic contact line passed through the plane $x = 0$, as discussed before. At large wrapping angles, however, the solution paths presented a turning point. There was always a speed ratio above which no two dimensional, steady-state solution could be obtained. The dynamic contact line position of the flow states presented in Figure 10 are shown in Figure 11.

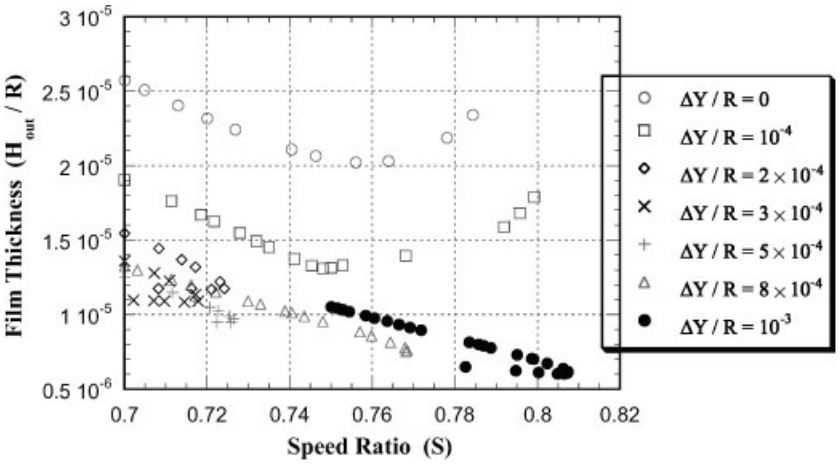

Figure 10. Thickness of metred film as a function of speed ratio and wrapping angle. $\mathrm{Ca} = 0.1$ and $\tau = 10^{-6}$.

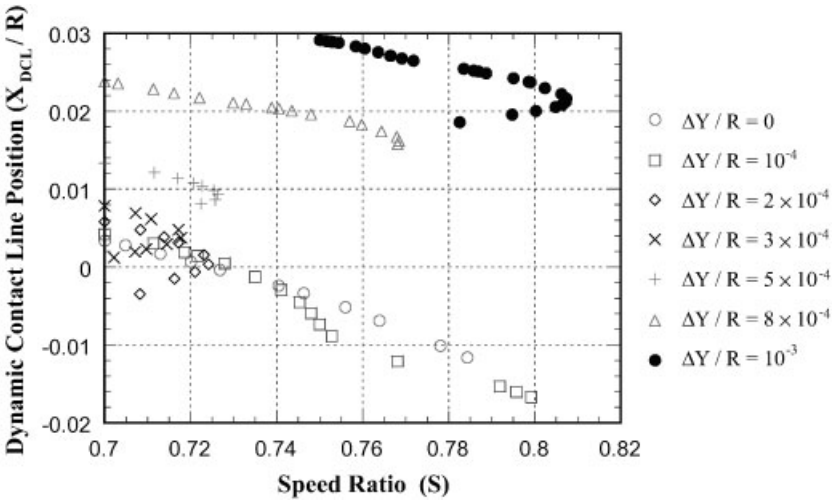

Figure 11. Dynamic contact line position as a function of speed ratio and wrapping angle. $\mathrm{Ca} = 0.1$ and $\tau = 10^{-6}$.

The movement of the contact line as the roll is pushed against the substrate has an important implication related with the seashore instability. As the wrapping angle rises, the contact line is pushed away from the $x = 0$ plane, delaying the onset of seashore instability. However, the presence of turning points in the solution path indicates that, above a critical speed ratio, the stable flow state is not two dimensional, but three dimensional with variations in the cross web direction. The metred film left on the roll breaks into stripes of liquid, generally called rivulets (see Reference [11]).

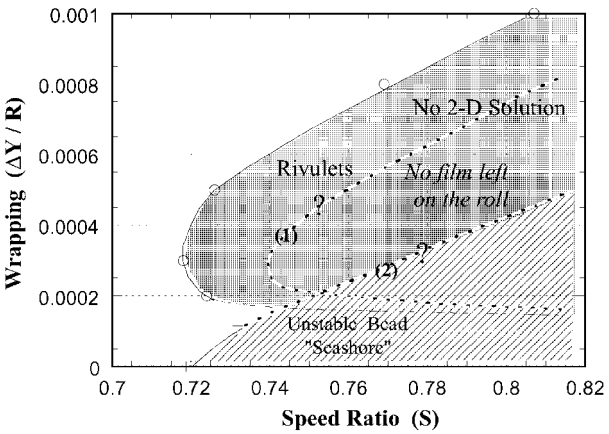

Figure 12. Coating window projection on the speed ratio vs wrapping angle plane. $\mathrm{Ca} = 0.1$ and $\tau = 10^{-6}$.

The theoretical predictions can be used to construct an operating window for this coating process, i.e. a diagram that shows the process condition as a function of wrapping angle and speed ratio. The speed ratio at which the turning point occurs is associated with the onset of rivulets. The speed ratio at which the dynamic contact line passes through the $x = 0$ plane is associated with the onset of seashore.

An example of such coating window is shown in Figure 12. The clear region represents the area of stable and two-dimensional flow. At small wrapping angles, there is a transition to an unstable (seashore instability), transversely continuous bead. At larger wrapping angles, there is a transition to discontinuous metred film, i.e. rivulets. The two-dimensional model described in this work can only predict these limits in the coating window. However, experimental evidence presented first by Satas [11] suggests that there should be a transition from a rivulet state to one at which the liquid film is completely transferred from the roll to a web, leaving the roll almost perfectly clean. This possible transition is represented by the dotted line labelled (1) in Figure 12. Another possible transition also represented in the figure is from a stable flow state with no metred film left on the roll to one at which the bead is unstable leading to a seashore type of defect—dotted line (2) in Figure 12.

Figure 13 presents experimental evidence of the flow transitions discussed before. It shows photographs of the coating bead, looked through the transparent web. First, at speed ratio $S = 0.75$, the metred film left on the roll is in the form of rivulets. As the speed ratio rises ($S = 1$), the rivulets disappear and the roll is virtually clean, without any visible liquid on it. As the speed ratio reaches $S = 1.25$, the coating bead becomes unstable, leading to a seashore defect on the substrate.

4. FINAL REMARKS

Tensioned web roll coating is used to produce very thin liquid layers at relative small cost. An important advantage of this method is that the film thickness and quality is fairly insensitive

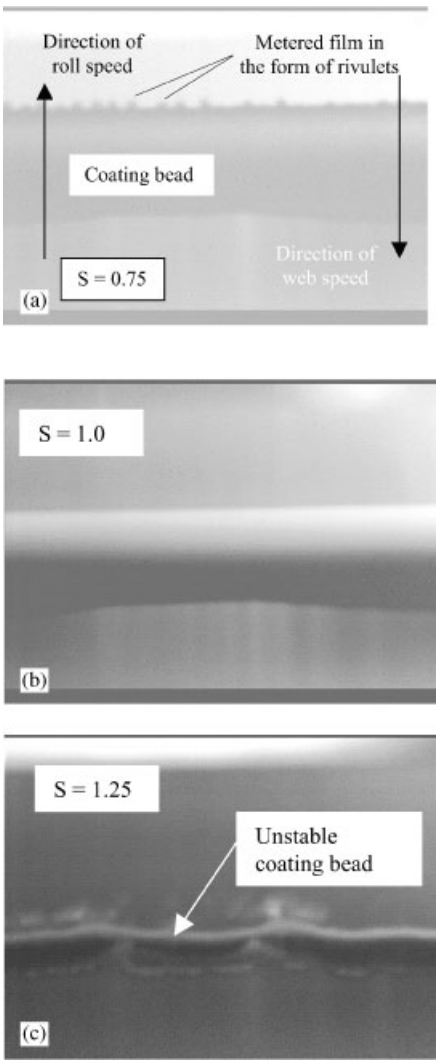

Figure 13. Flow visualization of coating bead at three different states: (a) three-dimensional flow with rivulets, (b) virtually no film left on the roll, and (c) seashore instability with no metred film left on the roll surface.

to mechanical tolerances. Despite its large industrial application, theoretical models of this process have been limited to simple lubrication analysis.

This work presented a theoretical approach to determine the operating window of the process operating in a reverse mode. The free surface liquid flow was described by the complete Navier–Stokes equations with the appropriate boundary conditions to account for the effect of surface tension. The deformation of the substrate was described by cylindrical shell approximation. The system of partial differential equations was solved by the Galerkin/finite element method.

The results show the operating conditions at which the metred film breaks into rivulets and the conditions at which the bead becomes unstable, leading to a coating defect known as seashore. These two limits of operation determined theoretically agree qualitatively with scarce experimental data available in the literature and with flow visualization presented here.

ACKNOWLEDGEMENTS

Part of this work was done when M. S. Carvalho was working with 3M Company. The final portion of it was supported by CNPq (Brazilian Research Council, Grant # 300242/98-0).

REFERENCES

1. Pranckh FR, Coyle DJ. Elastohydrodynamic coating systems. In *Liquid Film Coating*: *Scientifical Principals and their Technological Implications*, Kistler SF, Schweizer PM (eds). Chapman & Hall: London, 1997; 599–635.
2. Blok H, van Rossum JJ. The Foil Bearing: A new departure in hydrodynamic lubrication. *Lubrication Engineering* 1953; **9**:316–320.
3. Eshel A, Elrod HG. The theory of infinitely wide, perfectly flexible, self-acting foil bearing. *Journal of Basic Engineering* 1965; **87**:831–836.
4. Flügge W. *Stresses in Shells*. Springer: Berlin, 1960.
5. Kistler SF, Scriven LE. Coating flows. In *Computational Analysis of Polymer Processing*, Pearson JRA, Richardson SM (eds). Applied Science Publishers: London, 1983
6. Kistler SF, Scriven LE. Coating flow theory by finite element and asymptotic analysis of the Navier–Stokes system. *International Journal for Numerical Methods in Fluids* 1984; **4**:207.
7. Sakinger PA, Schunk PR, Rao RR. A Newton–Raphson pseudo-solid domain mapping technique for free and moving boundary problems: a finite element implementation. *Journal of Computational Physics* 1996; **125**:83–103.
8. De Santos JM. Two-phase cocurrent downflow through constricted passages. *Ph.D. Thesis*, University of Minnesota, 1991.
9. Coyle DJ, Macosko CW, Scriven LE. The fluid dynamics of reverse roll coating. *A.I.Ch.E. Journal* 1990; **36**:161.
10. Hao Y, Haber S. Reverse roll coating. *International Journal for Numerical Methods in Fluids* 1999; **30**:635–652.
11. Satas D. *Web Processing and Converting Technology and Equipment*. Van Nostrand Reinhold: New York, 1984.

